ELSEVIER

Journal of Chromatography A, 756 (1996) 219–232

JOURNAL OF CHROMATOGRAPHY A

Characterization and impact of the temporal behavior of the electroosmotic flow in capillary isoelectric focusing with electroosmotic zone displacement

Lone Steinmann[a], Richard A. Mosher[b], Wolfgang Thormann[a,*]

[a]*Department of Clinical Pharmacology, University of Bern, Murtenstrasse 35, 3010 Bern, Switzerland*
[b]*Center for Separation Science, University of Arizona, Tucson, AZ 85721, USA*

Received 23 May 1996; revised 4 July 1996; accepted 9 July 1996

Abstract

A computer model permitting the combined simulation of the temporal behavior of electroosmosis and electrophoresis under constant voltage or current conditions and in a capillary which exhibits a pH dependent surface charge has been constructed and applied to the description of capillary isoelectric focusing with electroosmotic zone displacement (cIEF). Electroosmosis for each column segment is calculated based upon the voltage gradient and a wall titration curve (mobility vs. pH) which takes into account the dissociation (pK) of surface groups of the inner capillary wall, a wall mobility at full dissociation (high pH) and the non-vanishing surface charge at low pH. Then, the net electroosmotic flow is taken to be the average of all of the segment flows and considered to represent a plug flow. For a titration curve with pK around 6, a wall mobility around $7 \cdot 10^{-8}$ m^2/Vs and a residual mobility of about $1.2 \cdot 10^{-8}$ m^2/Vs at low pH, qualitative agreement between simulation data and experimental data obtained with an untreated fused-silica capillary is obtained. With the sample initially occupying 25% of the column length, electroosmosis is predicted to decrease four to six-fold during the course of the run. Simulation data further reveal (i) that the gradually displaced equilibrium gradient defined by the carrier ampholytes represents the main contributor (pump) to electroosmosis and (ii) that the entire cIEF process is characterized by the asymptotic formation of a stationary steady state zone configuration in which anionic electrophoretic transport and cathode electroosmotic zone displacement are opposite and of equal magnitude. The ampholyte pattern is predicted not to completely leave the capillary at its cathodic end. The position of the stationary boundary between the anolyte and the most acidic ampholyte is dependent on the residual electroosmotic flow at low pH and is thus defined by the composition of the anolyte and the most acidic carrier ampholytes. Having an untreated fused-silica capillary, 10 mM H_3PO_4 as anolyte and a sample occupying 25% of the initial column length the boundary is predicted to be immobilized at about 92% of the column length.

Keywords: Isoelectric focusing; Computer simulation; Electroosmosis; Electroosmotic zone displacement; Proteins; Caffeine

1. Introduction

Recently, principles and applications of capillary isoelectric focusing (cIEF) with electroosmotic zone displacement, a one-step procedure in which no mobilization of the separated ampholytes is required after focusing, have been described [1–12]. In the cIEF method developed in our laboratory [4–6,10,11] uncoated open-tubular fused-silica capillaries of 50–75 μm I.D. are employed. The capillary

* Corresponding author.

0021-9673/96/$15.00
PII S0021-9673(96)00627-9

is first flushed with the catholyte which contains a small amount of a neutral hydrophylic polymer, such as methylcellulose (MC) or hydroxypropylmethylcellulose. The polymer partially adsorbs to the capillary wall and thereby provides dynamic capillary conditioning which reduces protein–wall interactions as well as the electroosmotic flow. The sample, composed of carrier ampholytes and amphoteric sample compounds, is hydrodynamically introduced at the anodic capillary end with the initial zone length occupying 10–50% of the capillary length. After power application two electrokinetic effects occur concurrently, namely the formation of a longitudinal pH gradient with the separation of the amphoteric compounds (isoelectric focusing), and, due to the negative surface charge of untreated fused-silica, the electroosmotic displacement of the entire pattern towards the cathode. Thus, with cathodic electroosmosis and on-column sample detection towards the cathodic capillary end, solutes are slowly swept past the point of detection with basic ampholytes reaching the detector before neutral and acidic compounds.

Electroosmosis in capillary electrophoresis is known to be dependent on pH and the electric field, parameters which vary strongly along the capillary under the conditions of cIEF [13]. After separation, the pH is increasing from anode to cathode thereby spanning up to 8 pH units, whereas the electric field is typically high around neutrality and low at the two extremes of the equilibrium gradient [13,14]. Thus, compared to capillary zone electrophoresis, cIEF represents a more complex configuration in which electroosmosis is anticipated to be invariant. In a previous investigation from our laboratory [6], cIEF in presence of time dependent or time independent imposed cathodic plug flow along the capillary was described by means of computer simulation. The dynamics of the formation of the pH gradient and the separation of the proteins could thereby be related to electroosmotic flow and capillary length. The temporal behavior of electroosmosis, however, could not exactly be elucidated. In the mean time, a dynamic computer model for simulation of open-tubular capillary electrophoresis which includes in situ calculation of electroosmosis was constructed and successfully applied to describe sample behavior in capillary zone electrophoresis [15] and capillary isotachophoresis [16]. With this model, electroosmosis is calculated with the use of a wall mobility, the voltage gradient and the degree of dissociation of the silanol surface groups of the capillary wall. To compute electroosmosis in buffers with pH>5.5, a wall pK of 6 and a wall mobility between 5 and $7 \cdot 10^{-8}$ m^2/Vs are required to provide simulation data which are in good qualitative agreement with experimental data. These input parameters are in agreement with titration curves, i.e. electroosmotic mobility vs. pH relationships, determined in fused-silica capillaries for that pH range [15]. For pH<5.5, however, experimentally determined electroosmotic data do not follow the titration curve of a single monovalent acid, i.e. a curve which asymptotically reaches zero at pH<pK−2. Thus, the model has been extended to account for surface charge at low pH, a prerequisite for the proper description of cIEF with electroosmotic zone displacement. In this paper, the temporal variation of electroosmosis and detector profiles for proteins and carrier ampholytes predicted by this model are compared with data obtained experimentally.

2. Theoretical aspects

Electroosmosis is calculated by computer simulation employing the dynamic computer model which has been described in detail previously [13,15]. In the interest of clarity, the major points are reviewed. The model is one dimensional and based upon the principles of electroneutrality and conservation of mass and charge. Isothermal conditions are assumed and relationships between the concentrations of the various species of a component are described by equilibrium constants. Component fluxes are computed on the basis of electromigration, diffusion and electroosmosis along the separation axis. Initial conditions which must be specified for a simulation include the distribution of all components, the diffusion coefficient and net charge–pH relationships of the proteins, the pK and mobility values of the buffer constituents, the magnitude of constant current density or constant voltage, the electroosmotic flow constants (see below), the duration of the current flow, the column length as well as its segmentation and the permeabilities of the ends of the separation

space. The program outputs concentration, pH and conductivity profiles as functions of time and allows the presentation of these data either as profiles along the column at specified time intervals or as data which would be produced by a detector at a specified column location, i.e. segment number. Furthermore, it permits the calculation of the magnitude and temporal variation of electroosmosis and current density (at constant voltage) or voltage (at constant current).

Electroosmosis is treated as plug flow and calculated in the following way. For each column segment i, an electroosmotic mobility is defined according to

$$\mu_i = \mu_0\{10^{(pH_i - pK)}/(1 + 10^{(pH_i - pK)})\} = \mu_0\alpha \quad (1)$$

where μ_0 is a specified wall or absolute electroosmotic mobility [15], pK is the pK_a value of silanol (pK of the wall), pH_i is the pH value of the solution in the capillary segment i and α is the degree of ionization of the wall which varies from 0 to 1. Thus, for each pair of wall pK and mobility an electroosmotic mobility vs pH titration curve is obtained. For a mobility value of $5\cdot10^{-8}$ m^2/Vs, calculated titration curves for pK 5 and 6 are presented in Fig. 1 as solid and broken lines, respectively. According to this approach, the electroosmotic mobility is asymptotically reaching zero at pH<pK−2 and μ_0 at pH>pK+2. Electroosmosis, however, has been shown not to vanish at low pH [15]. Thus, the model has been extended to correct for surface charge contributions not originating from the dissociation of the silanol groups. The corrected titration data shown in Fig. 1 have been constructed according to

$$\mu_i = \mu_0 \cdot \alpha + \mu_c(1 - \alpha) \quad (2)$$

where μ_c is a correcting mobility which is typically in the order of $1\cdot10^{-8}$ m^2/Vs [15]. The second term in Eq. (2) provides a mobility addition of μ_c at pH<pK−2 and becomes zero at pH>pK+2. For $\mu_c = 0$, Eq. (2) yields Eq. (1).

Electroosmosis in a segment becomes

$$v_{EOi} = \mu_i E_i \quad (3)$$

where μ_i is the electroosmotic mobility according to Eq. (2) and E_i is the voltage gradient of segment i. Finally, the net electroosmotic flow is calculated via [15]

$$v_{EO} = 1/n\sum_{i=1}^{n} v_{EOi} \quad (4)$$

where n is the number of column segments. The time dependence is given by the variability of the voltage gradient and pH. Thus, this simple approach requires μ_0, μ_c and the pK_a value of the wall as inputs and enables the combined simulation of the temporal variation of electroosmosis and electrophoresis across the entire pH range, i.e. without restriction to pH values above 5 as was the case with the previous model based upon Eq. (1) [15].

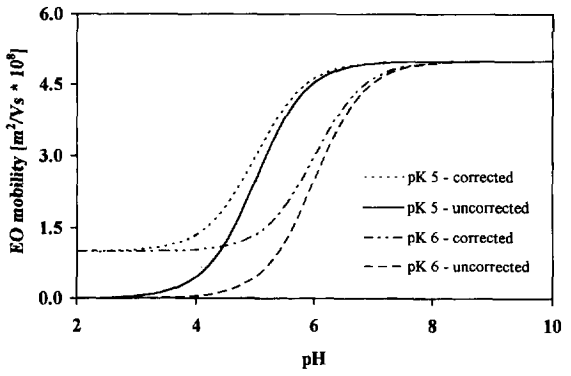

Fig. 1. Wall titration curves according to Eqs. (1,2) for two pK values (5 and 6), a wall mobility of $5\cdot10^{-8}$ m^2/Vs and, for correction at low pH (Eq. (2)), a mobility μ_c of $1\cdot10^{-8}$ m^2/Vs.

3. Experimental

3.1. Chemicals, electrolytes and sample

All chemicals employed were of analytical grade. Cytochrome c from horse heart (CYTC, M_r 12 384, pI 9.3) and MC (4000 cps) were purchased from Sigma (St. Louis, MO, USA). Ferritin from horse spleen (FER, M_r 450 000, pI 4.2–4.5) and equine myoglobin from horse skeletal muscle (MYO, M_r 17 800, pI 6.8–7.0) were from Serva (Heidelberg, Germany). Ampholine (pH 3.5–10) was obtained from Pharmacia-LKB (Uppsala, Sweden). If not stated otherwise, the experiments were performed using 20 mM NaOH containing 0.015% or 0.03% (w/v) MC as catholyte. During the runs, cathodic and anodic electrode vials were filled with 20 mM

NaOH and 10 m*M* H_3PO_4, respectively, solutions which did not contain any neutral polymer. The sample consisted of 0.19 mg/ml CYTC, 0.33 mg/ml MYO, 0.42 mg/ml FER and 4.5% (w/v) Ampholine. Proteins were dissolved in water. A solution containing 0.20 mg/ml caffeine in catholyte was used to determine the electroosmotic flow during an experiment.

3.2. Instrumentation and running conditions

The apparatus used was a BioFocus 3000 capillary electrophoresis system (Bio-Rad Laboratories, Hercules, CA, USA) controlled by an AST AT 386 computer system featuring the BioFocus 3000 Control Program Software (version 4.00) and the BioFocus 3000 Integrator Software (version 3.01). It was equipped with an untreated 50 μm I.D. capillary of 50 cm (45.4 cm) total (effective) length (Polymicro Technologies, Phoenix, AZ, USA) which was mounted into the user-assembled cartridge (Bio-Rad). If not stated otherwise, experiments were performed at a constant voltage of 20 kV and the cartridge and carousel temperatures were kept at 35 and 25°C, respectively. For the simultaneous monitoring of carrier ampholytes and proteins, electropherograms were concurrently registered at 210 and 280 nm. New capillaries were sequentially flushed with 1 *M* NaOH, 0.1 *M* NaOH and water for at least 20 min each and with a pressure of 100 psi (1 psi = 6894.76 Pa). Between runs the capillary was flushed at high pressure (100 psi) with 0.1 *M* NaOH (3 min), water (3 min) and catholyte (10 min). At the beginning of each day, the capillary was first rinsed with 1 *M* NaOH for 5 to 10 min. If not stated otherwise, sample injection was effected via application of 82 psi/s (at a pressure level of ~5 psi). For the estimation of electroosmosis during focusing five small caffeine pulses produced by 1 psi/s injections of the caffeine solution between 50 psi/s plugs of catholyte prior to sample injection (82 psi/s) and one caffeine peak thereafter (1 psi/s), were used.

3.3. Computer simulations

The cIEF separation of CYTC, MYO and FER in a pH 3–12 gradient formed by ten ampholytes between phosphoric acid and sodium hydroxide was simulated. If not stated otherwise, a 3 cm separation space divided into 600 segments of equal length, 25% initial occupation of the sample at the anodic capillary end and a constant voltage of 10 V (initial current density: 48.2 A/m^2) were used. A wall p*K* between 5 and 6, a wall mobility between 4 and $7 \cdot 10^{-8}$ m^2/Vs and a correcting mobility at low pH $\leq 1.5 \cdot 10^{-8}$ m^2/Vs were employed. The electrochemical input data of low molecular mass components, as well as the net charge–pH relationships and diffusion coefficients of the proteins, were the same as employed previously [6]. Ten hypothetical biprotic carrier ampholytes were used to establish a pH gradient between phosphoric acid and sodium hydroxide. The p*I* values uniformly span the range 3–12 ($\Delta pI = 1$). For each ampholyte, ΔpK was 2, the ionic mobility was $3 \cdot 10^{-8}$ m^2/Vs and the initial concentration was $2 \cdot 10^{-3}$ M. The concentrations of phosphoric acid and sodium hydroxide were 10 and 20 m*M*, respectively. The concentration of the three proteins in the sample zone was 0.05 m*M* each. The program was executed on an Excel AT 486 computer (Walz Computer AG, Bern, Switzerland) running at 50 MHz.

4. Results and discussion

4.1. Simulation of electroosmosis during focusing

Using the BioFocus 3000 and 40 m*M* phosphate buffers, the observed capillary titration data presented previously [15], including the steep mobility change in the pH 5 to 6 interval, could be confirmed (data not shown). With the addition of 0.015% (w/v) MC to the test solutions electroosmotic mobilities were determined to decrease in the order of 5–10%. Furthermore, electroosmosis at low pH was determined to be around $1 \cdot 10^{-8}$ m^2/Vs [15]. Thus, based upon previous experience with capillary zone electrophoresis [15] and capillary isotachophoresis [16], a wall p*K* value between 5 and 6, a wall mobility around $5 \cdot 10^{-8}$ m^2/Vs and a correcting mobility μ_c of $1 \cdot 10^{-8}$ m^2/Vs were chosen for simulation. Typical titration data of the capillary wall are presented in Fig. 1.

The simulation data presented in Fig. 2 were obtained under a constant 10 V employing a wall p*K*

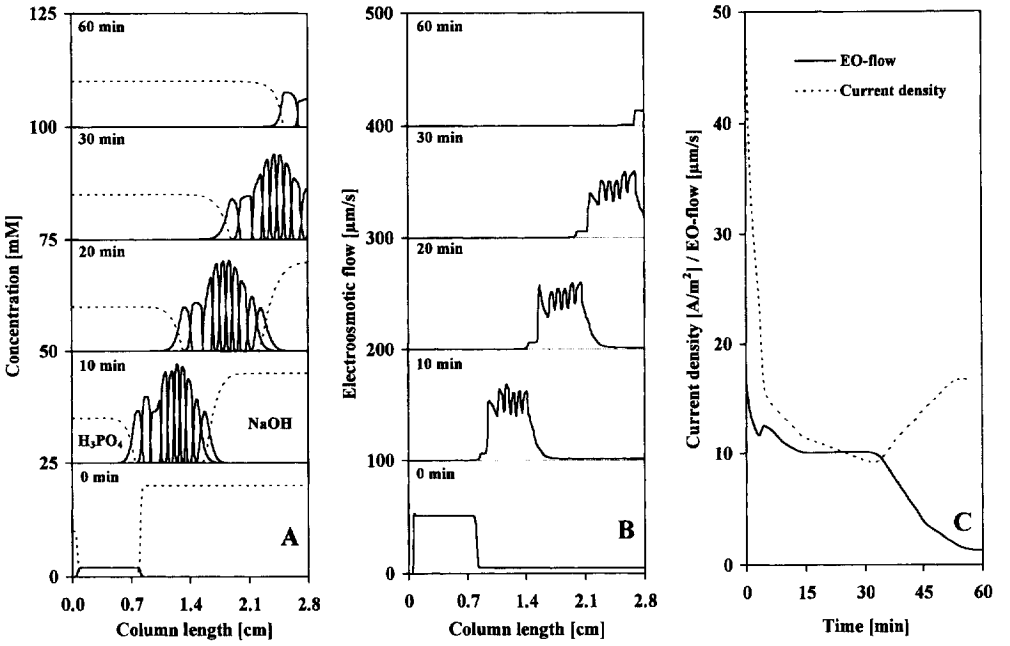

Fig. 2. Computer simulated (A) concentration profiles of the carrier ampholytes (solid lines), anolyte (H_3PO_4, broken line to the left) and catholyte (NaOH, broken line to the right) at specified time points after power application, (B) electroosmotic flow distributions at the same time points, and (C) temporal behavior of the net electroosmotic flow and current density. For the sake of presentation, the distributions shown in panels A and B are plotted with a *y*-axis offset of 25 m*M* and 100 µm/s, respectively. The data were generated at constant voltage of 10 V and with a wall p*K* of 5 and a wall mobility of $5 \cdot 10^{-8}$ m^2/Vs (titration data represented by the solid line of Fig. 1). The cathode is to the right. The distributions of the proteins are not shown.

of 5 and a wall mobility of $5 \cdot 10^{-8}$ m^2/Vs (titration data given by the solid line in Fig. 1). Concentration profiles for the ampholytes, phoshoric acid (anolyte) and NaOH (catholyte) at 0, 10, 20, 30 and 60 min after power application are presented in panel A. Within the first 10 min, focusing of the carrier ampholytes is shown to be complete (for a description of the entire separation process, including the dynamics of the proteins, refer to Refs. [6,13]). Furthermore, at that point in time the entire pattern is predicted to have almost completely moved out of the initial sample region. After 30 min of current flow, NaOH is depicted to have left the capillary at its cathodic end. As time goes on, almost the whole pattern is predicted to leave the column. Analysis of the data between 40 and 50 min revealed a gradual formation of a stationary steady state zone formation in which the boundary between phosphoric acid and the most acidic ampholyte becomes immobile at about 82% of the column length (refer to top graph in panel A of Fig. 2). In this configuration electrophoretic displacement of the ampholyte towards the anode and electroosmotic zone displacement are opposite and of equal magnitude. This stationary steady state is comparable to that predicted for anionic isotachophoresis [16]. In isoelectric focusing, anolyte and catholyte can destabilize the separative pattern continuously and rapidly by an isotachophoretic mechanism in which anolyte and catholyte act as leaders such that carrier ampholytes at the extremes are migrating away from the focused zone pattern [13,17]. This effect is also seen in the simulation data presented in panel A of Fig. 2. In the case of the anolyte, $H_2PO_4^-$ is the leading anion. Its physico–chemical properties and concentration determine the velocity of the anionic, isotachophoretic train of the most acidic carrier compounds [17]. In the stationary steady state, this electrophoretic transport towards the anode and electroosmosis towards the cathode are of equal magnitude.

The data presented in panel B of Fig. 2 represent electroosmotic flow data predicted for each capillary

segment after 0, 10, 20, 30 and 60 min of current flow. These profiles do not reflect a real, physical distribution, but provide insight into the pumping activity of each zone. The contribution of the catholyte to electroosmosis is shown to be low. The same applies to the most acidic carrier ampholytes whereas all other ampholytes contribute significantly to electroosmosis. Thus, the conclusion can be reached that the ampholyte pattern is the main contributor to the electroosmotic flow in cIEF. It is important to realize that with the titration curve employed, the anolyte does not contribute to electroosmosis at all.

The temporal behavior of the current density and the net electroosmotic flow are shown in panel C. Electroosmotic zone displacement is predicted to decrease from an initial value of ~16.3 μm/s, to have a characteristic bump after 4.5 min, to stabilize at ~10 μm/s between 15 and 32 min and to further decrease and level off thereafter. The current density is decreasing steeply from the initial value of 48.2 A/m^2 to ~15 A/m^2 within the first 5 min. Thereafter a much slower decrease and commencing at ~33 min a marked increase are predicted (dotted line in Fig. 2C). It should be noted that the bump in the electroosmotic flow and the bend in the current graph after ~5 min were found to coincide with the time required to completely focus the ampholyte pattern (data not shown). The gradual loss of the ampholyte pattern at the cathodic capillary end is shown to result in a marked decrease (increase) of the electroosmotic flow (current density). After ~55 min, these properties become constant (1.31 μm/s; 17.4 A/m^2), this indicating the formation of a stationary steady state zone distribution.

The data presented in Fig. 3 were obtained under the same conditions as those employed to generate the data of Fig. 2, except that the whole simulation was performed under a constant current density of 15 A/m^2. At this current level, a comparable overall displacement rate of the focusing pattern and the establishment of the same stationary steady state configuration are predicted. This is clearly seen via comparison of panels A of Figs. 2 and 3. However, the temporal behavior of electroosmosis is not the same (panels C). With constant current density, the initial value (5.07 μm/s) is considerably smaller compared to that predicted for constant voltage (16.3 μm/s). Then, electroosmosis is predicted to increase with time until the focused carrier ampholytes are

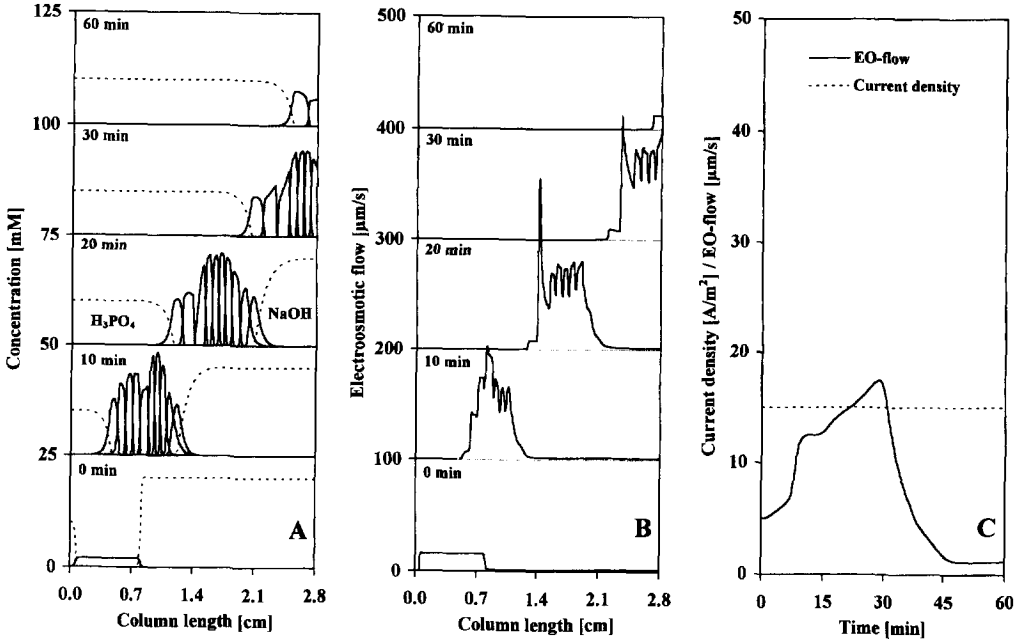

Fig. 3. Computer simulated data obtained at constant current density of 15 A/m^2 under otherwise identical conditions as for Fig. 2.

starting to leave the column. From then on, electroosmosis is predicted to decrease strongly and level off at 1.15 μm/s. Comparison of panels B of Figs. 2 and 3 further reveals that the pumping activity within the carrier ampholytes is initially smaller under the selected constant current conditions. With time, however, it becomes larger compared to that predicted under constant voltage (Fig. 2).

The location of the equilibrium gradient is best visualized by looking at pH and conductivity data. The data presented in Fig. 4A represent these properties predicted by constant voltage simulation for one time point (10 min of current flow) and using a wall pK of 5 and a wall mobility of 5×10^{-8} m^2/Vs. As expected, a stepwise pH increase from that of the anolyte to the value of the catholyte is predicted. Furthermore, conductivity is depicted to be low across the gradient and high within anolyte and catholyte. Thus, the high electric field across the gradient (see also Ref. [14]) provides the force field required for the substantial electroosmotic pumping within this region. The titration curve used in the simulations presented in Figs. 2 and 3 is based upon protolysis of the silanol groups only. It therefore reaches zero at low pH (Fig. 1, solid line). From the experimental electroosmotic mobility determinations it was observed, however, that this was not the case in reality. At low pH the capillary was determined to exhibit a residual mobility which is attributed to contributions made by anion adsorption. In order to obtain the right contribution to electroosmosis at low pH, the titration curve was optimized by the use of a correcting mobility $\mu_c = 1\cdot10^{-8}$ m^2/Vs (dotted line in Fig. 1). The influence of this mobility correction on the electroosmotic pumping activity of each fluid element in the capillary is depicted in Fig. 4B. It is clearly seen that the acidic part of the ampholytes (anode to the left) contributes more to the electroosmotic flow when the correction is employed. This is even more pronounced for a configuration with a wall pK of 6 and without changing the wall mobility parameters (Fig. 4C, titration data of Fig. 1). Furthermore, introduction of $\mu_c > 0$ provides electroosmotic pumping for the anolyte.

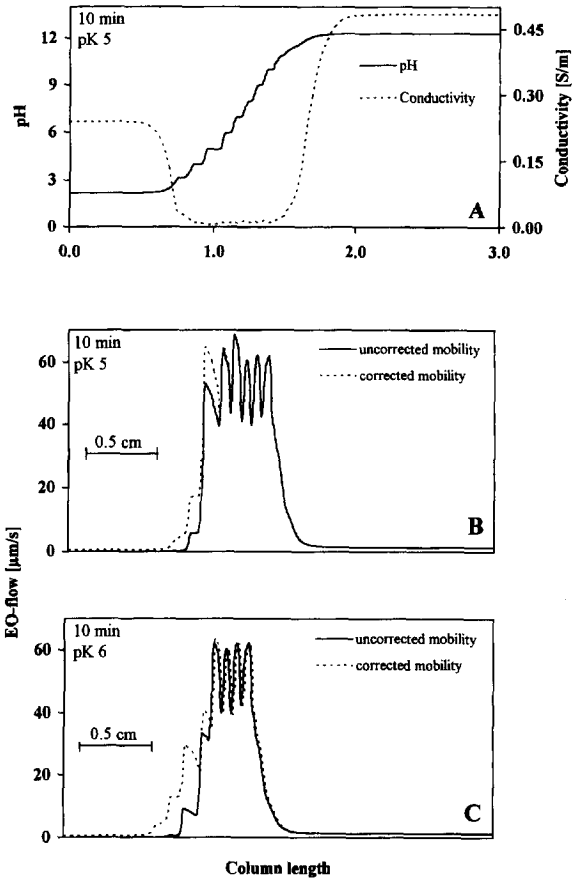

Fig. 4. Computer simulated (A) pH and conductivity profiles after 10 min at constant voltage and pK 5 (conditions of Fig. 2), (B) electroosmotic flow distribution for the same time point with $\mu_c = 0$ (solid line) and with $\mu_c = 1\cdot10^{-8}$ m^2/Vs (broken line), and (C) the same as in panel B but for pK 6. For the sake of comparison, the electroosmotic flow distributions predicted with the mobility correction at low pH in panels B and C were shifted along the x-axis such that distributions overlapped at the cathodic end.

The impact of the use of the different wall titration data on the predicted net electroosmotic flow, the current density and detector profiles obtained with a sensor located at 60% column length are shown in panels A to C, respectively, of Fig. 5. For all four cases whose data are displayed, the overall shape of the temporal behavior of the net electroosmotic flow (panel A) is predicted to be similar. It is noteworthy, that the flow level reached at equilibrium (about 60 min of current flow) is predicted to be largely independent of the wall pK. Its value, however, becomes larger with an increase of μ_c, the correcting mobility for low pH. Furthermore, the model predicts equal current levels for the first 30 min and the establisment of different current plateaus thereafter

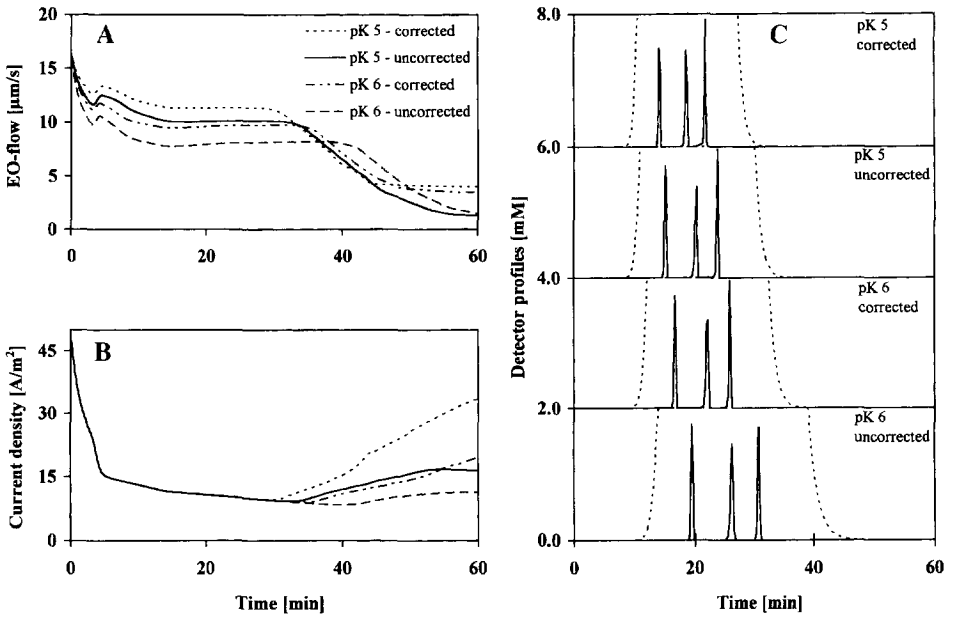

Fig. 5. Computer predicted (A) temporal behavior of the net electroosmotic flow, (B) the temporal variation of the current density and (C) detector profiles for a detector located at 60% of column length obtained under constant voltage conditions and with the four wall titration curves depicted in Fig. 1. The data presented in panel C correspond to those which would be seen with an absorbance detector operated at 280 nm (proteins; solid line) and 210 nm (carrier ampholytes of which the two edges are depicted only; broken line).

(panel B). Finally, the stationary boundary between anolyte and the most acidic carrier ampholyte was predicted to be dependent on the correction employed for electroosmosis at low pH. With $\mu_c = 1 \cdot 10^{-8}$ m^2/Vs, the stationary boundary was determined to be at 92% of column length (data not shown), this representing a significant difference to the 82% predicted for $\mu_c = 0$ (Fig. 2A).

The best approach for validation of the temporal, computer predicted zone distributions would be some sort of an array sensor capable of visualizing all zone boundaries along the capillary at any given time after current application. Having electrophoretic instruments with a single, stationary absorbance detector, however, indirect experimental validation is also possible. Accordingly, computer predicted detector profiles for a detector positioned at 60% of column length are presented in panel C of Fig. 5. Data for two wavelengths (e.g. for 210 and 280 nm depicted as dotted and solid lines, respectively) were generated by summation of the concentrations of carrier ampholytes and proteins, respectively. As discussed before [6], the three proteins are shown to be well separated when detection is effected at 60% column length. Furthermore, detection times of proteins and carrier ampholytes are dependent on the wall titration data employed. Detection times are predicted to be dependent on both, wall pK and μ_c, the mobility for correction at low pH. Corrected titration data provide faster runs compared to those with $\mu_c = 0$. Furthermore, lowering of the wall pK value results in an increase of electroosmotic transport towards the cathode.

4.2. Experimental data

Experimental cIEF data with the three test proteins are presented in Fig. 6 and Fig. 7. The data depicted are those obtained at 280 nm (solid line) and 210 nm (dotted line). At the former wavelength proteins are monitored whereas at the lower wavelength carrier ampholytes can be visualized. The cIEF data shown in panel A of Fig. 6 were obtained in presence of caffeine pulses. Caffeine is a neutral solute within the entire pH range [18] and can thus be employed (i) to mark the position of the focused ampholyte

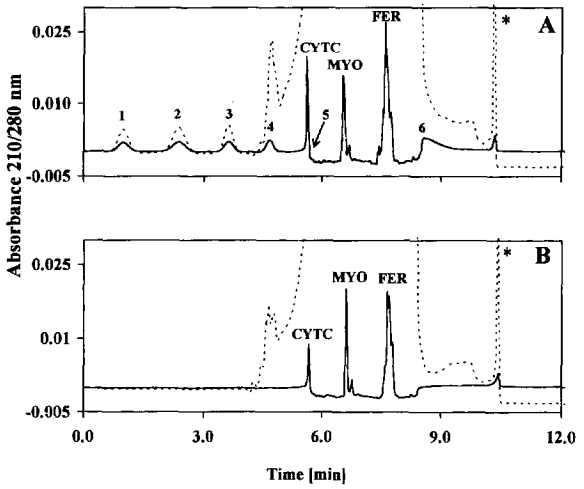

Fig. 6. cIEF electropherograms monitored at 280 nm (solid line) and 210 nm (broken line) with CYTC, MYO and FER as model proteins (A) in presence of six caffeine pulses and (B) without caffeine as marker substance. The asterisk marks the end of the carrier ampholytes.

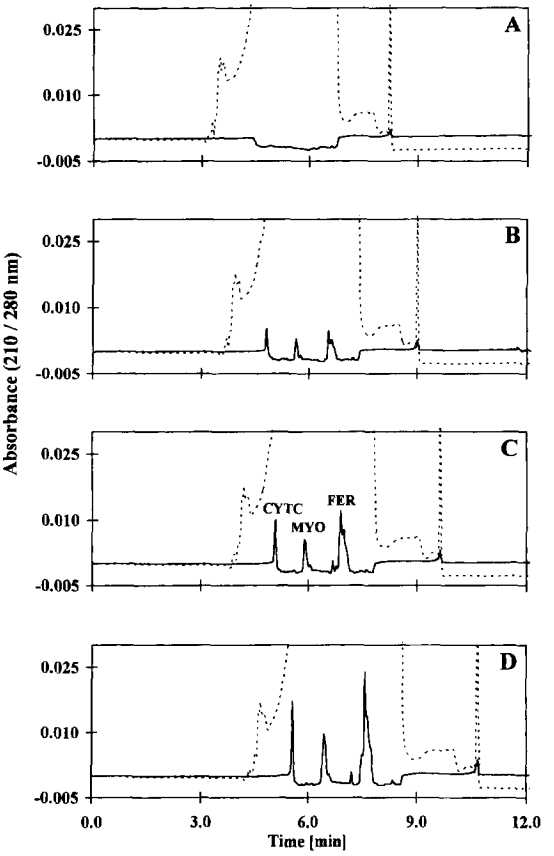

Fig. 7. cIEF electropherograms obtained (A) without proteins, (B) with a 1/3 protein load, (C) with a 2/3 protein load and (D) with the protein sample under otherwise identical conditions as for Fig. 6B.

pattern and (ii) to assess the magnitude of the electroosmotic flow. The experimental determination of electroosmosis will be discussed in the third part of this chapter. In the data presented, 6 caffeine pulses were introduced with pulses five and six being located at either end of the sample zone. Pulse 5 was determined to coelute with CYTC (blank data not shown) and therefore mark the cathodic front edge of the initial sample zone. The carrier ampholytes detected before pulse 5, i.e. essentially between pulses 4 and 5, represent those which began to isotachophoretically migrate towards the cathode prior to detection. This behavior is marginally seen in the simulation data presented in Figs. 2 and 3 and has been completely described previously in absence of electroosmosis [13,17]. Furthermore, caffeine pulse 6 and the sharp peak denoted by an asterisk mark the end of the focused carrier ampholytes and the front of the anodically migrating ampholytes, respectively. The behavior of the most acidic ampholytes is illustrated by the simulation data presented in Figs. 2 and 3 (for details refer to Refs. [13,17]). The conclusion can be drawn that the time period during which a decreased detector response at 280 nm is monitored (Figs. 6 and 7) represents the time period during which the fluid plug initially occupied by the sample is swept across the point of detection.

The data shown in panel B of Fig. 6 were monitored on a separate day and without the caffeine pulses. Comparison of the electropherogram with that presented in panel A provides insight into the reproducibility obtained. Not surprisingly, caffeine appears not to disturb the eluting characteristics of the focusing pattern. However, conditioning of the capillary was recognized as the key issue for reproducibility. Typically, observed run times strongly decreased during the first three runs on a measuring day. This could somewhat be eliminated by first rinsing with 1 *M* NaOH for at least 10 min. Optimized running conditions (cf. Section 3) were determined to be comparable to those reported

previously for another instrumental configuration [5]. With the sample whose data are depicted in panel A of Fig. 6, R.S.D. values for detection times and peak areas of the three proteins were determined to be on the 2 to 4% levels ($n=3$). Other conditioning procedures studied were characterized by two- to three-fold higher R.S.D. values.

Although reproducible results were obtained for blank and the three-protein sample, the presence of the three proteins was found to retard the cathodic displacement of the focusing zone pattern. Without proteins, the ampholyte pattern was detected earlier (panel A of Fig. 7). It was interesting to realize, that CYTC and MYO (at the protein levels employed here; cf. Section 3) did not change the eluting behavior of the cIEF pattern (data not shown). However, FER was found to be responsable for the reduction of electroosmosis. It appears, that column conditioning with 0.03% MC cannot prevent deleterious interactions of FER with the capillary walls. Furthermore, retardation of the zone pattern was determined to be dependent on the protein load. With increasing amount of the three proteins and unchanged initial sample length, detection times increased (Fig. 7). Thus, electroosmosis became significantly lower as the protein load was increased. Furthermore, data obtained with different initial sample lengths (injections between 50 and 165 psi/s instead with 82 psi/s) exhibited increased complexity due to the variability of the protein load (data not shown).

The data presented in Fig. 8 represent the focusing currents observed during the runs whose electropherograms are shown in Fig. 7. For all cases, currents are shown to first decrease, then increase and level off, phases which are in agreement with computer prediction (see above). Without proteins, the final (steady state) current is shown to reach the highest plateau. With increase of the protein load, a decrease in the current plateau was observed. The current is dependent on column resistance and independent on the magnitude of the plug flow. Thus, the variability of the current plateaus observed suggest that different stationary zone configurations are established. Since electroosmosis increases as the FER load is decreased (Fig. 7), it appears that with higher flow along the capillary a smaller part of the acidic carrier ampholytes remains in the capillary, this resulting in increased steady state current levels.

4.3. Comparison of simulation and experimental data

The experimental validation presented here is based on the data depicted in Figs. 6 and 7 for which a 50 cm capillary with ~25% initial sample zone length, a constant voltage of 20 kV, and a detector location at about 90% of column length were employed. Using this setup, electroosmotic mobilities in presence of catholyte (20 m*M* NaOH at pH 12.3) were determined to be 7.30 and $6.99 \cdot 10^{-8}$ m^2/Vs without and in presence of 0.015% MC, respectively. Corresponding values for the anolyte (pH:2.21) were found to be 1.20 and $1.13 \cdot 10^{-8}$ m^2/Vs, respective-

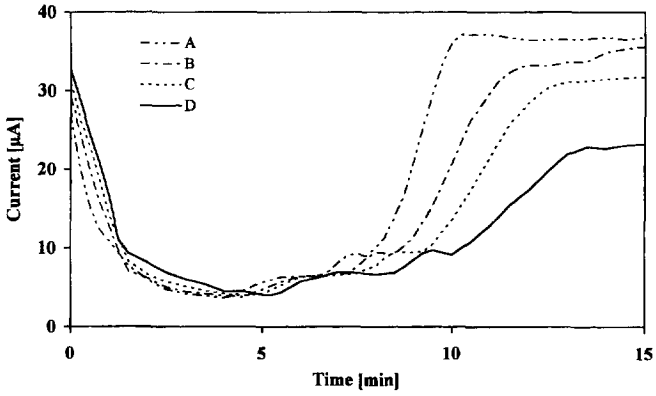

Fig. 8. Experimentally monitored currents for the cIEF runs whose data are depicted in panels A to D of Fig. 7.

ly. Thus, for comparison of simulation data and experimental data without proteins (Fig. 7A), simulations were performed with a wall mobility of $7 \cdot 10^{-8}$ m^2/Vs, a correcting mobility μ_c of $1.2 \cdot 10^{-8}$ m^2/Vs and using pK values of 5 and 6. The data presented in panels A to C of Fig. 9 represent computer predicted data for the temporal behavior of electroosmosis, the variation of current density and emulated detector profiles for a detector positioned at 90% of column length, respectively. Furthermore, simulation data obtained with pK 6, a wall mobility of $5 \cdot 10^{-8}$ m^2/Vs and $\mu_c = 1.5 \cdot 10^{-8}$ m^2/Vs are also shown. For close comparison of simulation and experimental data, the following has to be considered. In the experiment, a voltage gradient of 400 V/cm was applied, this being 120 times larger than that employed for simulation. On the other hand, the column length used for computer prediction was 16.67 fold shorter compared to that used experimentally. Thus, time scales of prediction and experimental validation should be comparable when the simulation time scale is divided by 7.20, the ratio of the two scaling numbers. As is shown with the data presented in Fig. 9C and 9D, this was found to be essentially true. Furthermore, for the sake of data comparison, computer predicted electroosmotic flow and current density data were multiplied by 120.

In the simulation data obtained with pK 5, mobility $7 \cdot 10^{-8}$ m^2/Vs and $\mu_c = 1.2 \cdot 10^{-8}$ m^2/Vs carrier ampholytes (and proteins, top graph in panel C of Fig. 9) were predicted to be swept across the point of detection at earlier time intervals as was the case experimentally. Good qualitative agreement was obtained via increase of the wall pK to 6 (center graph of Fig. 9C) and an even better fit was noted by reducing the wall mobility and increasing μ_c (bottom graph of panel C). The agreement reached is remarkable, particularly in the light of the differences between the carrier compounds used for simulation and experiment. Furthermore, the impact of the ionic strength on electroosmosis is not considered in the employed model. It is important to note, that there will always be a specific combination of the three input parameters with which simulation data will compare reasonably well with the experimental data. Nevertheless, it is assuring to realize that a wall pK

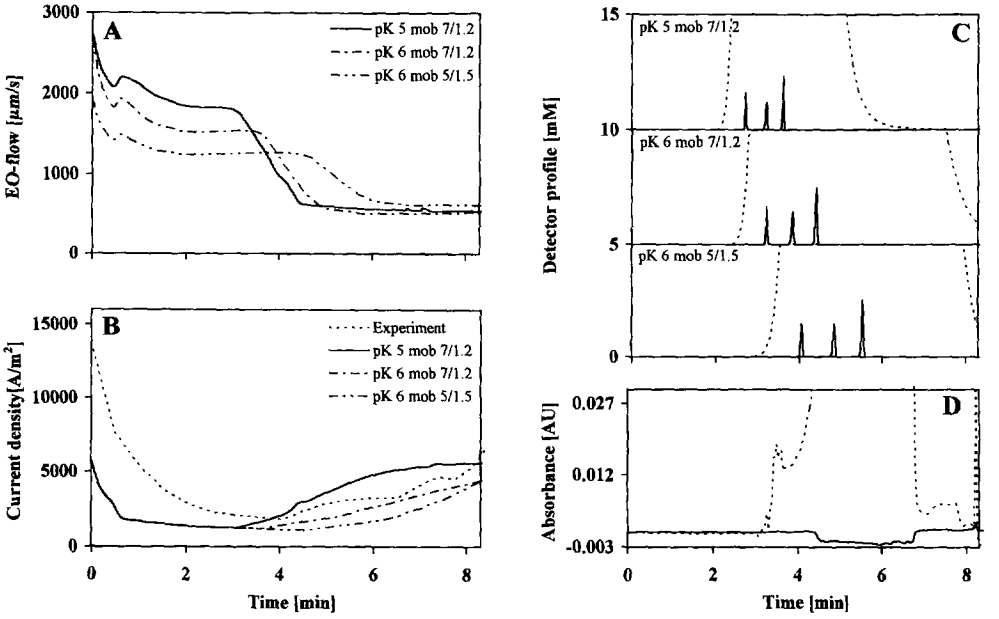

Fig. 9. Comparison of computer predicted and experimental data without the protein retardation effect. Converted simulation data (panels A to C), experimental current density (dotted line in panel B) and an electropherogram obtained without proteins (panel D) are shown. For further explanations refer to Section 4.3.

of 6 again produces good data as was the case in capillary zone electrophoresis [15] and capillary isotachophoresis [16].

The simulation data presented in Fig. 10 represent those which were generated for comparison with the experimental data in presence of the three proteins (Figs. 6A and 6B). Due to the reduction of electroosmosis caused by FER, simulation conditions other than those used to generate the graphs of Fig. 9 were employed. To reach qualitative agreement between simulation and experimental data, significantly lower values for wall mobility and μ_c compared to those used for matching the conditions without proteins (Fig. 9) had to be used. Reasonable good agreement was obtained with a pK of 6, a wall mobility of $4 \cdot 10^{-8}$ m^2/Vs and $\mu_c = 1.0 \cdot 10^{-8}$. Furthermore, the experimentally determined flow data were also found to reasonably agree with those predicted by the model (panel A of Fig. 10). The electroosmotic flow values were calculated with the detection times of the caffeine peaks (Fig. 6A) and the distances between them. The data points depicted in Fig. 10A represent the mean of four determinations (standard deviations smaller than diameter of filled circle).

Finally, the overall shape of the computer predicted and experimentally determined current density data appear to compare well (Figs. 9B and 10B). However, presumably due to the differences in carrier ampholytes employed for simulation and experimental validation, differences in magnitude of the current density were encountered.

5. Conclusions

With a wall titration curve comprising a pK of around 6, a wall mobility around $7 \cdot 10^{-8}$ m^2/Vs and a residual mobility of about $1.2 \cdot 10^{-8}$ m^2/Vs at low pH, qualitative agreement between simulation data and experimental data obtained with an untreated fused-silica capillary is obtained. Having a sample initially occupying 25% of the column, electroosmosis is predicted to decrease four to six-fold during the course of the run. Simulation data reveal that the

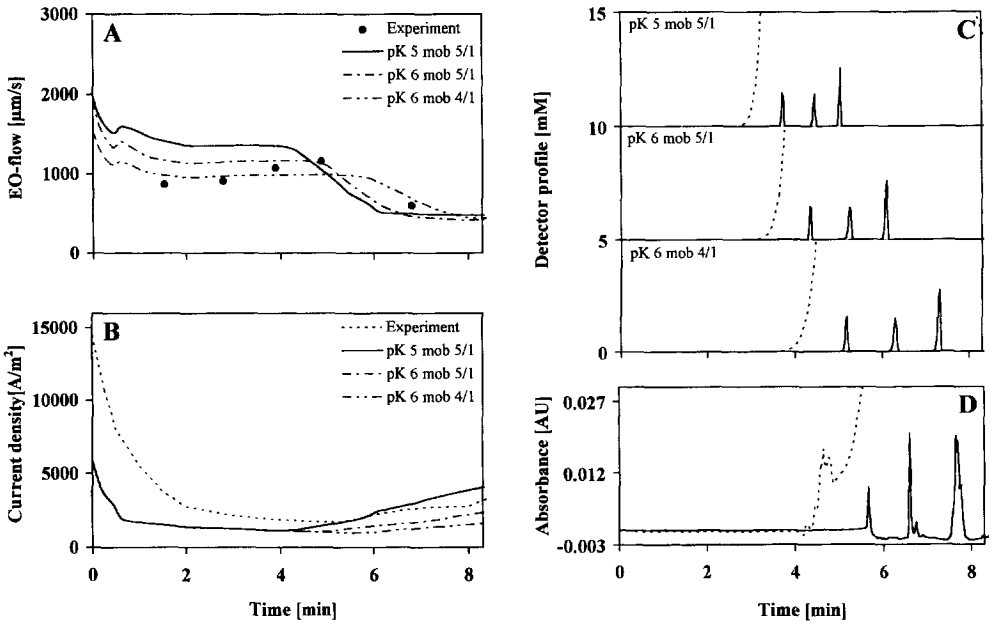

Fig. 10. Comparison of simulation and experimental data with protein retardation. Converted simulation data (panels A to C), experimental electroosmosis data (filled circles in panel A), experimental current density data (dotted line in panel B) and an electropherogram obtained with the three proteins (panel D) are shown. For explanations refer to Section 4.3.

gradually displaced equilibrium gradient defined by the carrier ampholytes represents the main contributor (pump) to electroosmosis. The varying electroosmotic pumping activity along the capillary which produces microcirculation and thus zone broadening [19,20] does not inhibit the formation of the zone pattern. It appears that the restoring forces encountered in this focusing technique sufficiently limit the effect of zone broadening caused by the variation of the zeta potential. Electroosmosis is shown to be dependent on the load of FER in the sample, a protein which unfavorably interacts with the capillary wall and thereby reduces electroosmosis. For that case, qualitative agreement between simulation and experimental data has been obtained by lowering the simulation input parameters for the wall mobility and the residual mobility at low pH.

The amalgam between simulation and experimental data reveals that the entire cIEF process in the fused-silica capillary is characterized by the asymptotic formation of a stationary steady state zone configuration in which anionic electrophoretic transport and cathodic electroosmotic zone displacement are opposite and of equal magnitude. The ampholyte pattern is predicted not to completely leave the capillary at its cathodic end. Simulation data reveal the position of the stationary boundary between the anolyte and the most acidic ampholyte to be dependent on the electroosmotic flow at low pH, i.e. on the properties and concentration of the anolyte and the most acidic carrier compounds. The position of the most anodic stationary boundary is independent on the selected wall pK and mobility at full dissociation. All three input parameters, however, are shown to influence the time interval at which the stationary steady state is attained. Having a fused-silica capillary, 10 mM H_3PO_4 as anolyte and a sample composed of 10 hypothetical biprotic carrier ampholytes whose pI values uniformly span the 3 to 12 range and which is occupying 25% of the initial column length, the boundary is predicted to be immobilized at about 92% of the column length. Without electroosmosis within the anolyte, immobilization of this boundary occurs at 82%. Despite there is a difference between the carrier ampholytes employed for simulation and experimental validation, there is remarkable qualitative agreement between theoretical prediction and experiment. Using the BioFocus with detection at about 90% of the column length, the entire cIEF pattern could be monitored even in presence of the electroosmotic flow retarding protein FER (Figs. 6 and 7). Furthermore, the variability of the steady state currents observed for the different protein loads (Fig. 8) indicate that different steady state zone structures are established. Inefficient rinsing occasionally lead to incomplete detection of the cIEF pattern. Furthermore, electroosmosis at low pH (anolyte has a pH value of 2.21) is difficult to control experimentally. Thus, for cIEF with electroosmotic zone displacement, detectors should be located before 92% of column length. Further work, including the improvement of the computer model to consider the impact of the ionic strength on electroosmosis, is in progress.

Acknowledgments

The authors gratefully acknowledge the generous loan of a BioFocus 3000 from its manufacturer, Bio-Rad Laboratories, Life Science Group, Hercules, CA. This work was sponsored by the Swiss National Science Foundation.

References

[1] J.R. Mazzeo and I.S. Krull, Anal. Chem., 63 (1991) 2852.
[2] J.R. Mazzeo and I.S. Krull, J. Chromatogr., 606 (1992) 291.
[3] J.R. Mazzeo and I.S. Krull, J. Microcol. Sep., 4 (1992) 29.
[4] W. Thormann, J. Caslavska, S. Molteni and J. Chmelík, J. Chromatogr., 589 (1992) 321.
[5] S. Molteni and W. Thormann, J. Chromatogr., 638 (1993) 187.
[6] W. Thormann, S. Molteni, E. Stoffel, R.A. Mosher and J. Chmelík, Anal. Methods Instrumentation, 1 (1993) 177.
[7] X.-W. Yao and F.E. Regnier, J. Chromatogr., 632 (1993) 185.
[8] G.G. Yowell, S.D. Fazio and R.V. Vivilecchia, J. Chromatogr. A, 652 (1993) 215.
[9] J.R. Mazzeo, J.A. Martineau and I.S. Krull, Anal. Biochem., 208 (1993) 323.
[10] J. Caslavska, S. Molteni, J. Chmelík, K. Šlais, F. Matulík and W. Thormann, J. Chromatogr. A, 680 (1994) 549.
[11] S. Molteni, H. Frischknecht and W. Thormann, Electrophoresis, 15 (1994) 22.
[12] S. Kundu and C. Fenters, J. Cap. Electrophoresis, 2 (1995) 273.

[13] R.A. Mosher, D.A. Saville and W. Thormann, The Dynamics of Electrophoresis, VCH, Weinheim, 1992.
[14] W. Thormann, N.B. Egen, R.A. Mosher and M. Bier, J. Biochem. Biophys. Methods, 11 (1985) 287.
[15] R.A. Mosher, C.-X. Zhang, J. Caslavska and W. Thormann, J. Chromatogr. A, 716 (1995) 17.
[16] W. Thormann, J. Caslavska and R.A. Mosher, Electrophoresis, 16 (1995) 2016.
[17] R.A. Mosher and W. Thormann, Electrophoresis, 11 (1990) 717.
[18] C.-X. Zhang, F. von Heeren and W. Thormann, Anal. Chem., 67 (1995) 2070.
[19] J.L. Anderson and W.K. Idol, Chem. Eng. Commun., 38 (1985) 93.
[20] B. Potoček, B. Gaš, E. Kenndler and M. Štědrý, J. Chromatogr. A, 709 (1995) 51.